

Numerical simulation of the seismic response of the Zipingpu concrete face rockfill dam during the Wenchuan earthquake based on a generalized plasticity model

Degao Zou ^{a,b}, Bin Xu ^{a,b,*}, Xianjing Kong ^{a,b}, Huabei Liu ^c, Yang Zhou ^{a,b}

^aThe State Key Laboratory of Coastal and Offshore Engineering, Dalian University of Technology, Dalian 116024, China

^bInstitute of Earthquake Engineering, Dalian University of Technology, Dalian 116024, China

^cDepartment of Civil Engineering, City College of New York, NY 10031, United States

ARTICLE INFO

Article history:

Received 18 June 2012

Received in revised form 17 October 2012

Accepted 21 October 2012

Available online 17 December 2012

Keywords:

Generalized plasticity model
Zipingpu CFRD
Wenchuan earthquake
Crushing damage
Joint dislocation
Settlement

ABSTRACT

The strong ground motion of the 2008 Wenchuan earthquake in China caused considerable damage to the Zipingpu concrete face rockfill dam (CFRD). The maximum crest settlement was approximately 1.0 m, and compressive failure and joint dislocations were observed in the face slabs. This damage has made it necessary to understand the damage pattern and safety of high CFRDs subjected to strong earthquake shaking, and the response of the Zipingpu CFRD during the Wenchuan earthquake can be used as a benchmark for this purpose. In this study, a 3D dynamic procedure was employed to simulate the dynamic responses of the Zipingpu CFRD. The rockfill materials were described using a generalized plasticity model, while the interfaces between the face slabs and cushions were modeled using zero-thickness interface elements that follow a perfect elasto-plastic stress-strain model in the tangential direction using Coulomb's friction law. Dam deformation, face-slab stress, and face joint dislocations were simulated, and the results were compared with the field measurements. Using the generalized plastic model, the residual deformation of the dam during the earthquake could be directly obtained without being complemented by separate, semi-empirical procedures. The rockfill materials shrank to the center of the valley due to the strong shaking, causing crushing damage in the zone of the slabs. The dislocation of construction joints was also duplicated by the numerical procedure. The results of this study indicate that a 3D finite element procedure based on a generalized plasticity model can be used to evaluate the dynamic responses of CFRDs during strong earthquakes.

Crown Copyright © 2012 Published by Elsevier Ltd. All rights reserved.

1. Introduction

A large earthquake ($M_s = 8.0$) occurred on May 12, 2008, in Wenchuan in the Sichuan Province of China, which is located approximately 17 km west of the Zipingpu concrete face rockfill dam (CFRD). The Zipingpu dam is the only CRFD (higher than 150 m) that has ever been subjected to such strong shaking, which caused obvious damage to the dam structure [1,2]. It is of great significance to the CFRD community to understand the damage pattern of this particular dam during the Wenchuan earthquake, and the response can also serve as a benchmark for the evaluation of CFRD safety during strong earthquakes. Although the damage to the Zipingpu dam has been summarized and analyzed according to field investigations, most of these summaries [1,2] focused on the phenomenon of the damage; few numerical studies have been

conducted to fully understand the damage to the Zipingpu dam and its causes.

Numerical analysis has been a well-accepted tool for the seismic safety evaluation of earth and rockfill dams. Mejia and Seed [3] compared the 2D and 3D dynamic responses of earth dams. Gazetas and Dakoulas [4] discussed the design principles and seismic defensive measures of earth-core dam and CRFD based on the case of an actual rockfill dam in a narrow valley. Uddin and Gazetas [5] analyzed the high accelerations in the near-crest area of 2D CRFDs. A procedure for the dynamic analysis of CFRDs under strong shaking was proposed in a study by Uddin [6], in which an equivalent linear model was applied to the rockfill materials; the slab-rockfill interface was also considered. Elgamal et al. [7–9] used a sliding-block model to analyze the observed deformation and acceleration responses of the La Villita Dam, which was subjected to six major earthquakes. Recently, several researchers investigated the seismic behavior of CFRDs in narrow canyons using nonlinear 3D dynamic analysis [10,11]. Seiphoori et al. [12] studied the effect of a spatially variable input excitation applied along a canyon boundary based on

* Corresponding author at: The State Key Laboratory of Coastal and Offshore Engineering, Dalian University of Technology, Dalian 116024, China.

E-mail address: xubin@dlut.edu.cn (B. Xu).

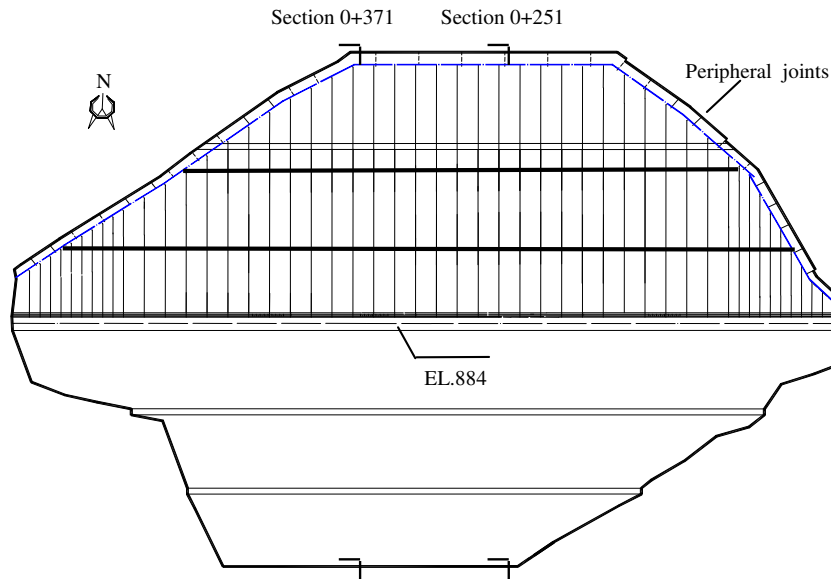


Fig. 1. Plan view of the Zipingpu CFRD.

a scaled boundary finite element method considering the scattered motion of P, SV and SH waves. Arici [13] studied the state of stress and slab cracking during long-term impounding and earthquake loading. After the Wenchuan earthquake, Zhu et al. [14] performed back analyses on the static and dynamic characteristics of the Zipingpu CFRD according to the site investigations. Kong et al. [15,16] performed equivalent linear analyses to study the damage mechanism and the seismic performance of the Zipingpu CFRD.

So far, the majority of the seismic finite element analyses of earth and rockfill dams assumed the equivalent linear behavior of soils [17]. This method is convenient and accepted by design engineers because of the extensive work conducted in the determination of the model parameters and the capacity to capture the dynamic properties of earth and rockfill dams when seismic excitation is modest. However, the equivalent linear analysis cannot be used to reasonably evaluate the seismic residual deformation of the dam, which is important for the seismic design of high CFRDs. To overcome this disadvantage, two approximate approaches have been used to evaluate the seismically induced residual deformation of embankment dams. One approach is the well-known Newmark sliding block analysis [18], and the other is the global deformation method based on the strain potential concept proposed by Serff et al. [19]. However, neither of these approaches can properly estimate the residual volumetric compression of rockfill materials.

Nonlinear elasto-plastic analysis of rockfill dams would better simulate the behavior of rockfill materials under dynamic loading. Among the elasto-plastic soil models, the generalized plasticity model [20,21] has been successful in modeling the behavior of sandy soils under cyclic loading, including both the deviatoric and volumetric responses. In the framework of generalized plasticity, yield and plastic potential surfaces are not directly specified. Instead, direction vectors are used, and the hardening rule is explicitly described by a hardening modulus function. Recently, several improvements to the generalized plasticity model have been proposed [22–25]. Pastor et al. [22] considered the incorporation of anisotropy, whereas Sassa and Sekiguchi [23] proposed the inclusion of principle stress rotation effects. In addition, Ling et al. [24,25] adopted pressure-level dependency and the critical state concepts.

Based on the work of Pastor et al. [22] and Ling and Liu [24], the generalized plasticity model for sandy soil was modified to better consider the pressure dependency of rockfill materials under monotonic and cyclic loading conditions. The modified generalized

plasticity model [26] was used successfully to simulate the deformation of the Zipingpu CFRD during the construction and impounding processes.

In this study, the modified generalized plasticity model for rockfill materials was adopted to investigate the seismic responses of the Zipingpu CFED subjected to loading from the Wenchuan earthquake. Dam deformation and the slab stress during the Wenchuan earthquake were numerically simulated and compared with the field measurements. The causes of slab damage were analyzed based on the numerical simulation results. The same numerical procedure in the accompanying study [26] was used to obtain the initial conditions for the seismic analysis, considering the reservoir level at the time of the earthquake.

2. Damage to Zipingpu dam during the Wenchuan earthquake

The Zipingpu CFRD is located in the southern section of the fault zone in the Longman Mountains between the Beichuan–Yingxiu town and Guanxian–Anxian faults. A general view and typical section of the Zipingpu dam is shown in Figs. 1 and 2. Detailed information about the dam has been previously provided by the authors [26]. The locations of the Zipingpu CFRD and the epicenter of the Wenchuan earthquake are indicated in Fig. 3. The dam was designed for an intensity of VIII (Chinese scale) with a peak ground acceleration (PGA) of 0.26 g. Although the ground motion observation network at the site failed to record the acceleration time history on the bedrock during the Wenchuan earthquake, the bedrock peak ground acceleration (PGA) was estimated to be greater than 0.5 g [27].

The Zipingpu CFRD was clearly damaged during the Wenchuan earthquake [2,3]. The maximum crest settlement was approximately 1.0 m, as shown in Fig. 4a. Crushing damage to the #23 and #24 slabs occurred from the dam crest to EL. 790 m at the center of the valley, as can be observed in Fig. 4b. Significant dislocation damage also occurred between the stages II and III slabs at EL. 850 m, as depicted in Fig. 4c and d.

3. Constitutive model

In this study, the modified generalized model was used for the rockfill materials, and a perfect elasto-plastic interface model with

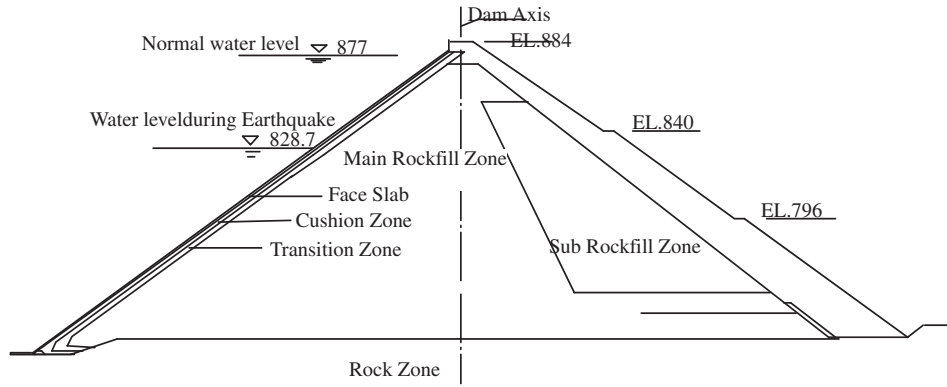


Fig. 2. 0 + 251 Typical section of the Zipingpu dam.

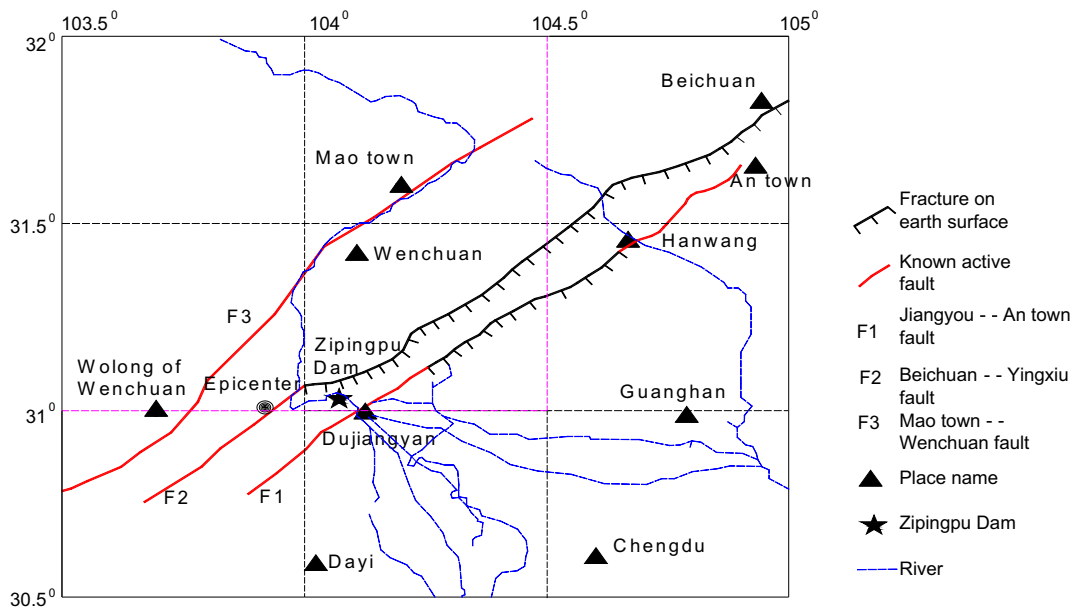


Fig. 3. Location of the Zipingpu dam and epicenter during the Wenchuan earthquake.

pressure-dependent shear stiffness was employed to simulate the interfaces between the face slabs and cushion gravel. Brief descriptions of these two constitutive models are provided in Appendices A and B, respectively.

4. Identification of parameters

4.1. Slabs

A linear elastic model was used to model the concrete face slabs. According to the available design information, the following properties were used in the analysis: density ρ of 2.40 g/cm³, modulus of elasticity E of 2.55e10 Pa, and Poisson's ratio ν of 0.167.

4.2. Rockfill materials

The rockfill material parameters are provided in Table 1 [26]. The model parameters are consistent with those used in the simulation of the static response of the Zipingpu CFRD, and the capacity of the constitutive model in describing the virgin loading, unloading and reloading responses of the Zipingpu rockfill material is demonstrated in the accompanying paper [26]. Fig. 5 presents a

comparison of the predicted and tested responses of the same rockfill material in a large-scale cyclic triaxial test.

4.3. Interface

The interfaces between the concrete slabs and cushion gravel were experimentally investigated by Zhang and Zhang [29,30]. The perfect elasto-plastic interface parameters were calibrated using their test results and are listed in Table 2. Fig. 6 compares the test results and the model predictions under cyclic loading. The compressive stiffness constant k_2 was set to 10,000 MPa/m to prevent interface penetration.

4.4. Slab joints and peripheral joints

The parameters of the slab joints and peripheral joints have not been reported in the literature. In this study, the compressive stiffness k_2 of the joints was assumed to be 25,000 MPa/m, which is equivalent to the compressive stiffness of the wood in the joints. The shear stiffness in the two shear directions was assumed to be 1 MPa/m. The parameters used in the dynamic analysis were consistent with those in the static simulation [26].

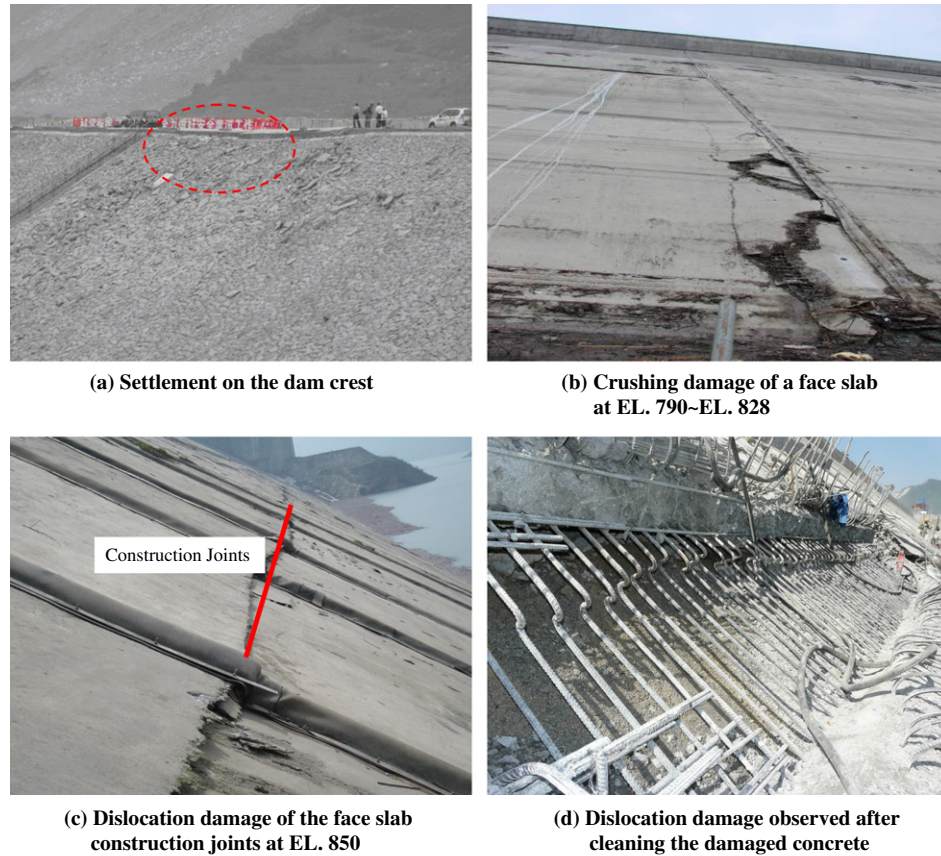


Fig. 4. Crest settlement and slab damage of the Zipingpu dam during the Wenchuan earthquake. (a) Settlement on the dam crest, (b) crushing damage of a face slab at EL. 790 ~ EL. 828, (c) dislocation damage of the face slab construction joints at EL. 850, and (d) dislocation damage observed after cleaning the damaged concrete.

Table 1
Rockfill material parameters in the modified generalized plasticity model.

G_0	K_0	M_g	M_f	α_f	α_g	H_0	H_{U0}	m_s
1000	1400	1.8	1.38	0.45	0.4	1800	3000	0.5
m_v	m_l	m_u	r_d	γ_{DM}	γ_u	β_0	β_1	
0.5	0.2	0.2	180	50	4	35	0.022	

4.5. Construction joints

In addition to the slab and peripheral joints, construction joints also existed between the different construction stages of the concrete face slabs. However, unlike the slab and peripheral joints, no water-stop materials were placed in the construction joints. In this study, the constructions were simulated based on the reduced shear strength of concrete. According to Hofbeck [31], the ratio of the shear strength to the compressive strength of concrete is between 0.119 and 0.316. In addition, Li et al. [32] reported the shear strength of concrete to be:

$$\tau_0 = \frac{1}{2} \cdot \sqrt{f_c \cdot f_t} \quad (1)$$

where f_c is the uniaxial compressive strength of concrete and f_t is the uniaxial tensile strength. This formula was used in the present study to calculate the shear strength of the face-slab concrete, and a value of 2.73 MPa was obtained according to the concrete grade ($f_c = 16.7$ MPa, $f_t = 1.78$ MPa).

A previous study demonstrated that the strength of concrete at the construction joints is only approximately 50% of that of the integral cast [33]. In addition, during seismic loading, the strength

of the concrete could decrease by up to 30% [34]. Therefore, the dynamic shear strength of the construction joints was assumed to be 0.545 MPa in the dynamic analysis and 1.365 MPa in the static simulation.

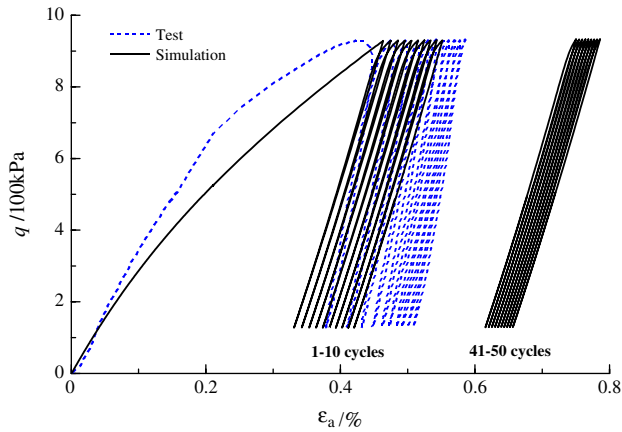
5. Finite element analysis

5.1. 3D finite element program

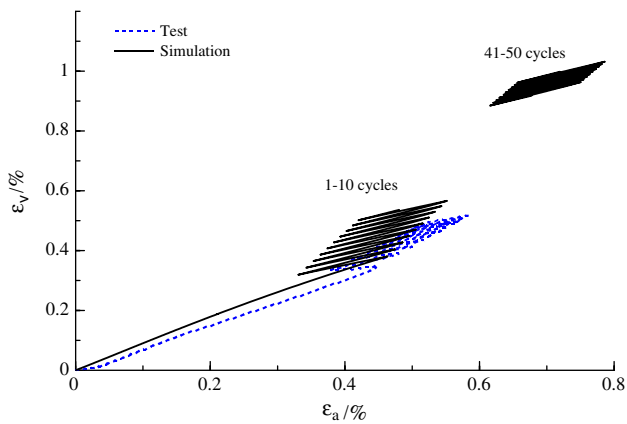
To properly capture the 3D dynamic responses of CFRDs [35], a 3D dynamic finite element code, namely Geotechnical Nonlinear Dynamic Analysis (GEODYNA), was developed by the first author using the object-oriented programming method [36], and the modified generalized plasticity model was incorporated into the code [26]. Construction simulation, seismic analysis and the stability analysis of geostructures can be performed using GEODYNA.

5.2. Finite element mesh

The same 3D finite element mesh of the Zipingpu CFRD used in the static simulation was adopted for the dynamic analysis [26]. In total, 23,994 elements were included in the mesh, including 614 slab elements. The rockfill materials and slabs were simulated using spatial eight-node isoparametric elements. The x , y and z directions at the bottom boundary of the dam were fixed. Finally, the hydrodynamic pressure acting on the face slabs was simulated in the dynamic analysis using the adding mass method [37], the mass element was defined by a single node, concentrated mass components. The simplified Westergaard formula was used and the added mass intensity on face-slabs can be expressed as



(a) The relationship between deviatoric stress and axial strain



(b) The relationship between volumetric strain and axial strain

Fig. 5. Comparison of model prediction and the test result of the rockfill material of the Zipingpu CFRD: (a) the relationship between deviatoric stress and axial strain and (b) the relationship between volumetric strain and axial strain.

Table 2
Parameters of the concrete-gravel interfaces of the Zipingpu CFRD.

k_1	k_2	n	φ	c
300	1e10	0.8	41.5	0

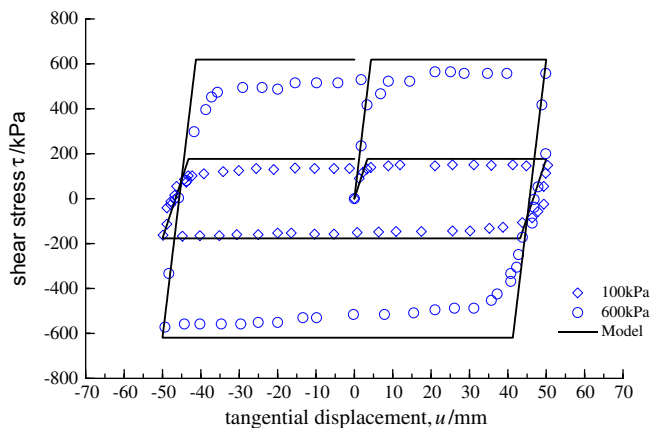
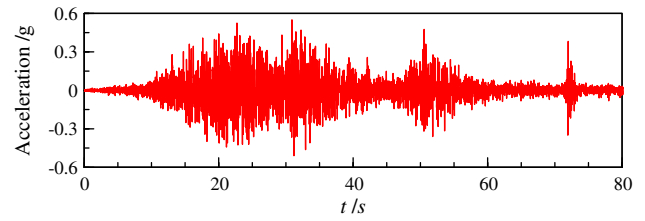
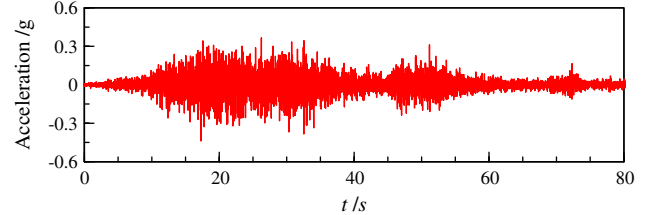


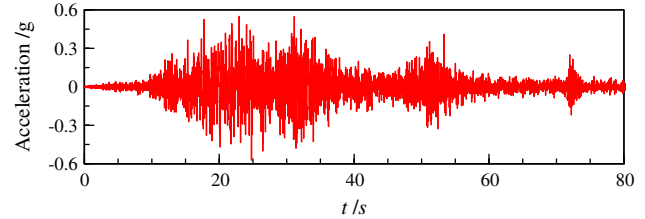
Fig. 6. Comparison of model predictions and test results of the stress–strain relationship of the concrete-gravel interfaces of the Zipingpu CFRD.



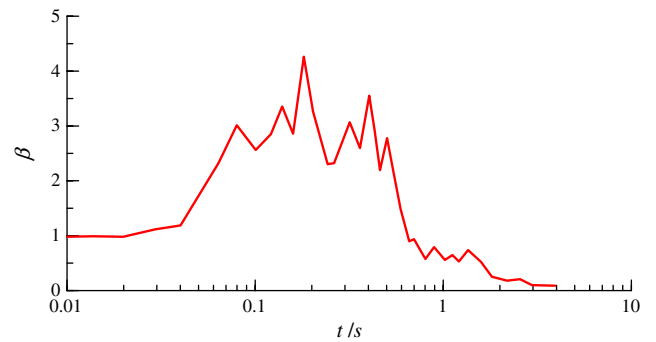
(a) Transverse direction



(b) Vertical direction



(c) Axial direction



(d) Acceleration amplification response spectrum

Fig. 7. Input earthquake motion. (a) Transverse direction, (b) vertical direction, (c) axial direction, and (d) acceleration amplification response spectrum.

$$m_{wi} = \frac{\varphi}{90} \cdot \frac{7}{8} \cdot \rho \cdot \sqrt{H_0 \cdot y_i}$$

where ρ is the water density, φ is angle of upstream slope, H_0 is depth from the position of node i to the bottom of reservoir, y_i is the depth from the position of node i to the surface of reservoir. During the dynamic analysis, the added mass under the water level during earthquake can be computed by integrating m_{wi} on the surface of face-slabs, there are 317 added mass elements totally.

5.3. Input ground motions

Because the ground motion observation network of the Zipingpu dam failed to record the acceleration time history on the bedrock during the Wenchuan earthquake, the bedrock acceleration time histories measured at Mao Town (located 75 km from the Zipingpu dam) were scaled to a peak value of 0.55 g [1]. These values were used as the horizontal input motions in the axial and transverse directions, which were applied at the bottom of the

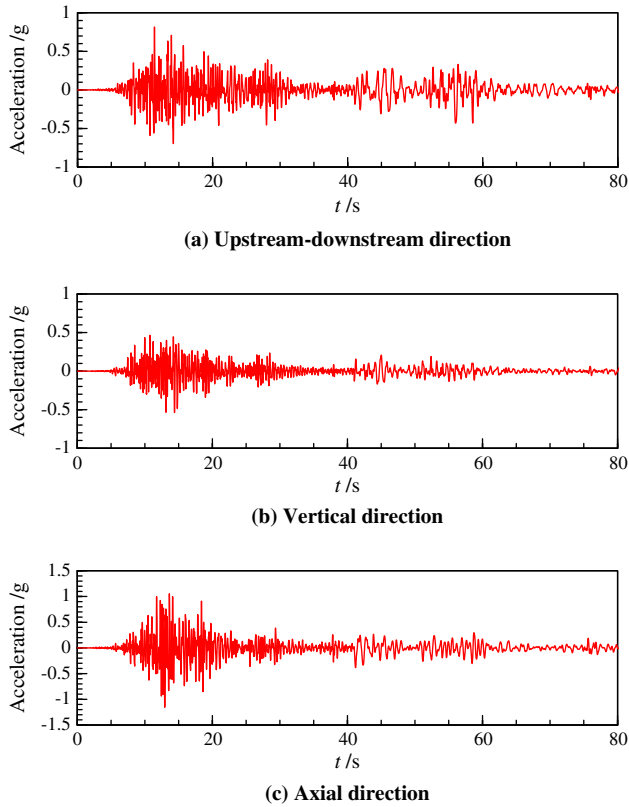


Fig. 8. Mid-crest absolute acceleration responses to the Mao Town seismic excitation scaled at 0.55 g: (a) upstream-downstream direction, (b) vertical direction and (c) axial direction.

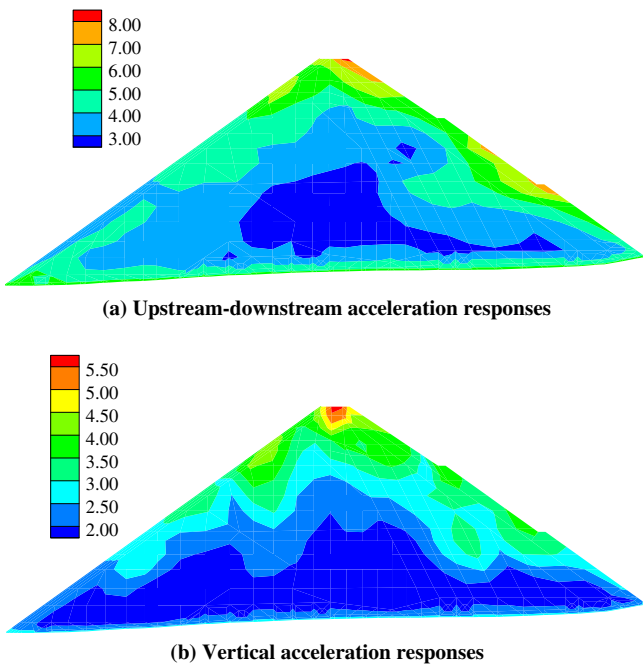


Fig. 9. The maximum acceleration responses of section 0 + 251 during earthquake (unit: m/s^2). (a) Upstream-downstream acceleration responses and (b) vertical acceleration responses.

mesh where the bedrock lies. The input acceleration time histories, together with the amplification response spectrum, are plotted in Fig. 7a–d. The predominant frequency of the input motion is

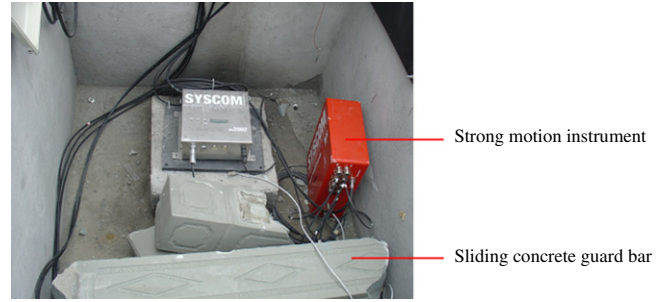


Fig. 10. Accelerometer on the dam crest and the fallen concrete guard column.

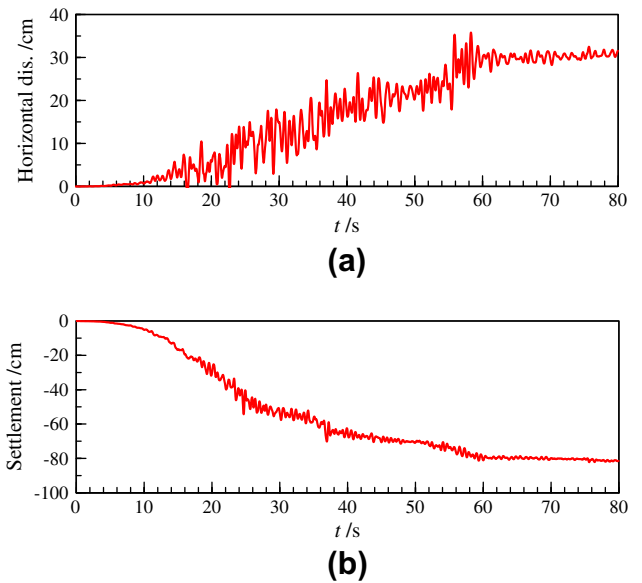


Fig. 11. Mid-crest displacement history of the Zipingpu dam during the earthquake: (a) upstream-downstream displacement and (b) settlement.

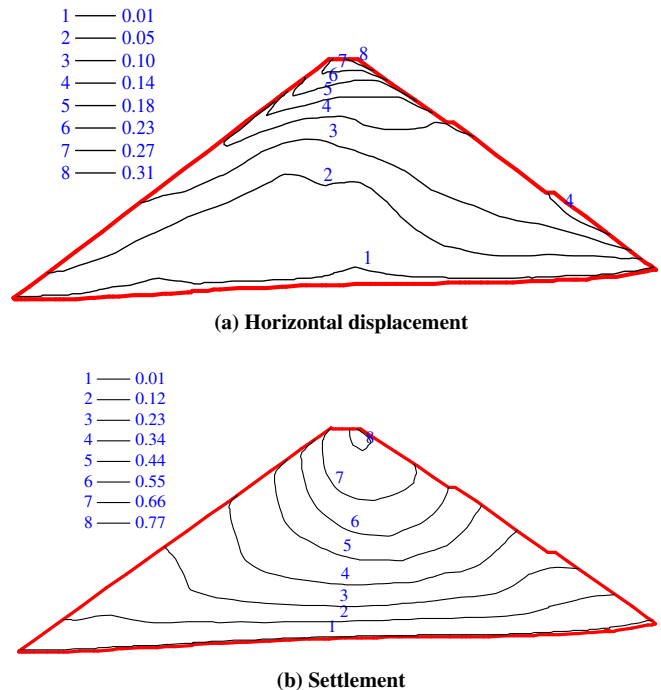


Fig. 12. Deformation of section 0 + 251 at the end of the earthquake (unit: m). (a) Horizontal displacement and (b) settlement.

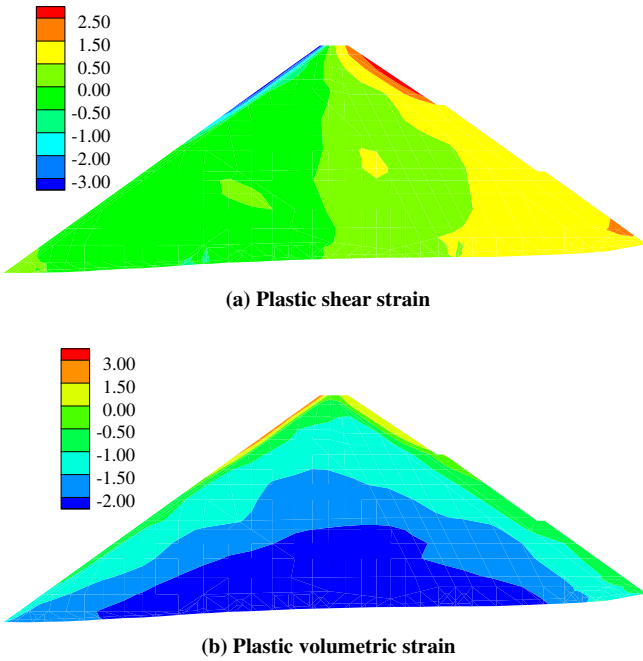


Fig. 13. Plastic strain of section 0 + 251 at the end of the earthquake (unit:%, volume shrink is negative). (a) Plastic shear strain and (b) plastic volumetric strain.

approximately 5.5 Hz. The vertical input motion was assumed to be 2/3 of the horizontal motion [16].

5.4. Damping

Similar to other hysteresis models for soils, the generalized plasticity model can capture the material damping at finite strain but predicts much smaller damping than that of actual soils at infinitesimal strain. Rayleigh damping was used to compensate for this deficiency. A viscous damping ratio of 5% was assumed for the rockfill materials [38]. The same damping ratio was also assumed for the concrete slabs.

6. Results and discussion

6.1. Acceleration response and deformation of the dam during the earthquake

The transverse, vertical and axial acceleration time histories at mid-crest are presented in Fig. 8a–c, with peak values of 0.82,

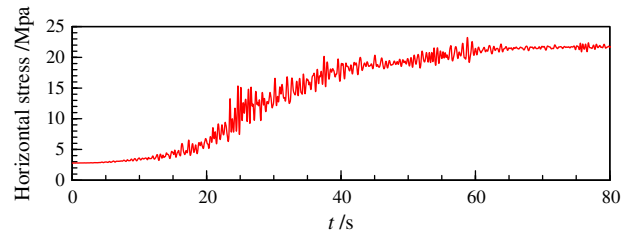


Fig. 15. Histories of stress in slab element at EL. 810 along the dam axial direction during the earthquake (compressive stress is positive, MPa).

0.54 and 1.15 g, respectively. The contour of the maximum acceleration responses of section 0 + 251 was illustrated as Fig. 9a and b, it indicated that the high peak accelerations developed in the mid-crest area of the dam, the distribution was similar to the results of Dakoulas by using equivalent linear method [11]. The measured peak accelerations on the crest exceeded 2.0 g during the Wenchuan earthquake [1,16]. However, the accelerometer was attached to concrete elements, and the very high accelerations may have been induced by the concrete guard column that fell during the shaking (Fig. 10) [15].

6.2. Deformation of the dam

The time histories of the horizontal crest displacement and the vertical settlement are plotted in Fig. 11. The settlement contours of the Zipingpu CFRD are illustrated in Fig. 12. The horizontal displacement (Fig. 11a) mainly developed in the downstream direction during the shaking, and the settlement gradually increased and reached 0.79 m at the end of the shaking. The shear strain and volumetric strain of section 0 + 251 at the end of the earthquake was given in Fig. 13. It can be seen that the shear strain exceeds 3% in the shallow slope area, which is consisted with the slope slide and slabs dislocation. Also, the volumetric strain illustrated a contraction trend in a wide area with higher confining pressure, and exhibited a dilatation trend in the shallow area.

A comparison of the measured and predicted residual settlements at cross section 0 + 251 is illustrated in Fig. 14. The predicted results exhibit a trend similar to that of the field measurement, and the maximum settlement occurred at the same location. In general, the numerical procedure was able to satisfactorily describe the deformation trends of the Zipingpu CFRD during the earthquake, indicating that the residual deformation of CFRDs during strong earthquake loading can be obtained directly from the numerical

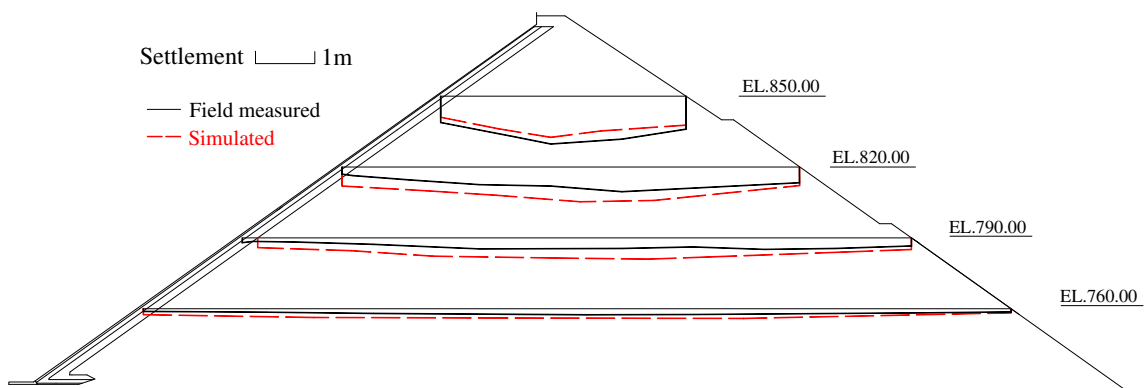


Fig. 14. Comparison of simulated and field-measured settlement of the dam section 0 + 251 at the end of the earthquake.

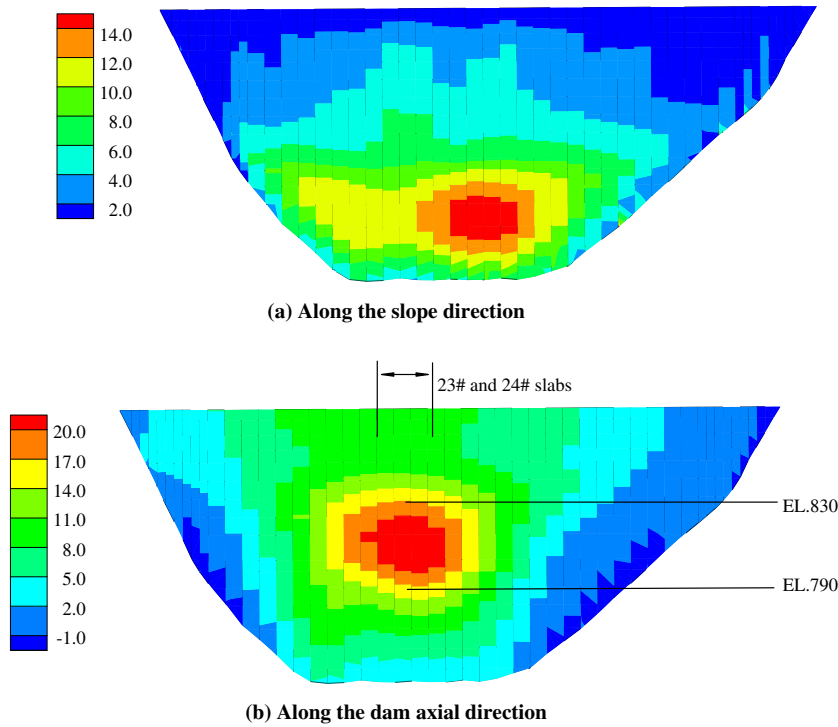


Fig. 16. Contour lines of stress in slab at the end of the earthquake (compressive stress is positive, unit: MPa). (a) Along the slope direction and (b) along the dam axial direction.



Fig. 17. The simulated dislocation distribution of the construction joints between the stages II and III slabs at the end of the earthquake.

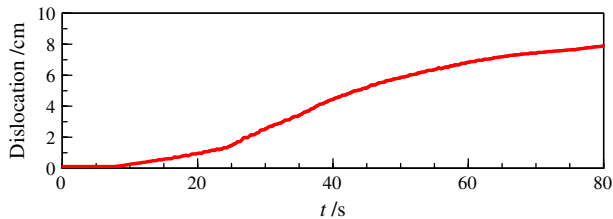


Fig. 18. The simulated dislocation history of the maximum construction joint element.

procedure used in this study rather than from the decoupled residual deformation model [19] to estimate permanent deformation after an earthquake.

6.3. Slab stress

After the Wenchuan earthquake, significant concrete crushing damage was observed in the #23 and #24 slabs (from EL. 790 to EL. 850 m). Based on the phenomena, it was postulated that the horizontal stresses in these slabs exceeded the compressive strength of the concrete ($f_c = 16.7$ MPa).

Fig. 15 shows the predicted stress developments during seismic loading in the slab elements, which are located in the area where concrete crushing was observed (where the tension stress is nega-

tive). The maximum compressive stress in the horizontal direction reached 22.0 MPa and occurred in the #23 and #24 slabs at EL. 810 m. During the earthquake loading, the rockfill materials shrank to the center of the valley, causing horizontal friction to the slabs, which resulted in large compressive stresses to the slabs in the area. Fig. 16 illustrates the contours of the slab stresses along the slope and the dam axis direction at the end of shaking. In slabs #22–#25 between EL. 790 and EL. 830, the compressive stresses along the dam axis exceeded 17.0 MPa. The tensile stress along the dam axis is no more than 1 MPa, and mainly distributed near the side slopes. In summary, the numerical simulation of the slab stresses agreed well with the observed slab damage during the earthquake.

6.4. Slab dislocation

During the Wenchuan earthquake, the reservoir water level was at 828.76 m, which was lower than the construction joint elevation (EL. 850 m) between the stages II and III slabs. The authors have investigated that water elevation has greater impact on the dislocation of face-slab during strong shaking based on Newmark slide method [41], and pointed out that the construction joint of face-slab is easier to dislocate with water elevation below the joint elevation. In this paper, the simulated dislocation distribution of the construction joints between the stages II and III slabs, at the end of the earthquake shaking, is illustrated in Fig. 17, and the maximum dislocation reached 7.98 cm. Fig. 18 reveals the development of the dislocation history of a typical construction joint element during earthquake shaking. The maximum simulated dislocation was less than the measured dislocation (17 cm). This result could be because only shear failure was considered in this study, while in reality, tensile damage may have contributed to the dislocation due to the separation of the slabs from the cushion layers.

7. Discussion and conclusions

The Zipingpu dam is the highest CFRD over 150 m to be subjected to strong earthquake shaking. This event provides a rare opportunity to verify the seismic design of and safety evaluation procedures for high CFRDs. The 3D dynamic response of the Zipingpu dam during the Wenchuan earthquake was simulated based on a modified generalized plasticity model for rockfill materials. The numerically simulated results were compared with the field measurements, and the following conclusions were drawn:

- (1) The modified generalized plasticity model is capable of describing the properties of rockfill materials under monotonic and cyclic loadings. It can be used for the dynamic response analysis of CFRDs.
- (2) Deformations of the Zipingpu CFRD during the Wenchuan earthquake were satisfactorily reproduced using the proposed numerical procedure. The residual dam deformation can be directly obtained from the 3D dynamic analysis instead of using a decoupled approach [19].
- (3) The rockfill materials shrank to the center of the valley during the earthquake shaking, inducing large compressive stresses in the slabs and resulting in crushing damage to the center slabs. Appropriate measures for controlling the horizontal stresses of slabs during earthquake loading may be necessary in the design of CFRDs.
- (4) The dislocation distribution of the construction joints between the stages II and III slabs was simulated, and the maximum dislocation value was 7.98 cm. The dislocation phenomenon that occurred during the Wenchuan earthquake was successfully captured by the proposed numerical procedure; however, the calculated magnitude was smaller than the measured magnitude. This discrepancy may have arisen from the linear elastic assumption of the concrete slabs and the simple shear failure model of construction joints employed in this study.
- (5) The possibility of considerable rockfill compression under high confining pressure and strong seismic loading may need to be considered in the seismic design of high CFRDs. At the same time, reinforcement at the construction joints should be enhanced to restrain the dislocation damage of the slabs.

Because measured bedrock motions were not available at the site, the earthquake shaking values used in this study may not be accurate. In addition, the rockfill dams were assumed to be fixed at the boundary with the bedrock, which led to seismic wave reflection and increased the seismic loading on the dam. However, the objective of this study was to reveal the deformation and damage mechanisms of the Zipingpu CFRD during the Wenchuan earthquake rather than to exactly match the response magnitudes. The proposed numerical procedure closely predicted the dam deformation trend, the development of large compressive stress in the slabs that were subjected to crushing damage, and the dislocation of the construction joints between the stages II and III slabs.

Acknowledgements

We would like to acknowledge the support provided by the State Key Program of the Natural Science Foundation of China (No. 51138001), the Science Fund for Creative Research Groups of the Natural Science Foundation of China (No. 51121005), the Natural Science Foundation of China (Nos. 51078061, 51279025, 50908032), and the Fundamental Research Funds for the Central Universities (Nos. DUT12LK37 and DUT11ZD110).

Appendix A

Generalized plasticity model for rockfill [21,26]

In plasticity theory, the strain increment can be decomposed into two parts:

$$d\boldsymbol{\varepsilon} = d\boldsymbol{\varepsilon}^e + d\boldsymbol{\varepsilon}^p \tag{1}$$

where $d\boldsymbol{\varepsilon}^e$ is the incremental elastic strain tensor and $d\boldsymbol{\varepsilon}^p$ is the incremental plastic strain tensor.

The stress–strain relationship is expressed as:

$$d\boldsymbol{\sigma}' = \mathbf{D}^{ep} : d\boldsymbol{\varepsilon} \tag{2}$$

In generalized plasticity theory, the elasto-plastic stiffness tensor is expressed as:

$$\mathbf{D}^{ep} = \mathbf{D}^e - \frac{\mathbf{D}^e : \mathbf{n}_g : \mathbf{n}^T : \mathbf{D}^e}{H + \mathbf{n}^T : \mathbf{D}^e : \mathbf{n}_g} \tag{3}$$

where $d\boldsymbol{\sigma}'$ is the incremental effective stress tensor; $d\boldsymbol{\varepsilon}$ is incremental strain tensor; \mathbf{D}^{ep} is elasto-plastic stiffness tensor; \mathbf{D}^e is elastic stiffness tensor; \mathbf{n} is loading direction vector; \mathbf{n}_g is flow direction vector; H is the plastic modulus.

The distinction between the loading and unloading directions is described using the following criteria:

$$\mathbf{n} : d\boldsymbol{\sigma}^e > 0 \quad (\text{loading}) \tag{4a}$$

$$\mathbf{n} : d\boldsymbol{\sigma}^e < 0 \quad (\text{unloading}) \tag{4b}$$

where $d\boldsymbol{\sigma}^e$ is the elastic stress increment.

The following generalized expression is proposed for the stress–dilatancy relationship [39]:

$$d_g = \frac{d\varepsilon_v^p}{d\varepsilon_s^p} = (1 + \alpha_g)(M_g - \eta) \tag{5}$$

where $d\varepsilon_v^p$ and $d\varepsilon_s^p$ are the incremental plastic volumetric and deviatoric strains, respectively. M_g is slope of the critical state line in the $p' - q$ plane, $\eta = q/p'$ is stress ratio, and α_g is a model parameter. M_g is related to the angle of internal friction at the critical state ϕ'_g and Lode's angle θ following the smoothed Mohr–Coulomb criterion proposed by Zienkiewicz and Pande [40]:

$$M_g = \frac{6 \sin \phi'_g}{3 - \sin \phi'_g \sin 3\theta} \tag{6}$$

The flow direction vector in triaxial space is then defined as:

$$\mathbf{n}_g^T = (n_{gv}, n_{gs})$$

with $n_{gv} = d_g / \sqrt{(1 + d_g^2)}$ and $n_{gs} = 1 / \sqrt{(1 + d_g^2)}$.

The non-associated flow rule is assumed in the model, and the loading direction vector is defined as:

$$\mathbf{n}^T = (n_v, n_s)$$

with $n_v = d_f / \sqrt{(1 + d_f^2)}$, $n_s = 1 / \sqrt{(1 + d_f^2)}$ and $d_f = (1 + \alpha_f)(M_f - \eta)$. Here, M_f and α_f are both model parameters.

The elastic behavior is defined by the shear and bulk moduli:

$$K = K_0 \frac{p'}{p'_0} \tag{7}$$

$$G = G_0 \frac{p'}{p'_0} \tag{8}$$

where K_0 and G_0 are the elastic volumetric and shear moduli, respectively, p' is the mean effective stress, and p'_0 is a reference value.

The plastic modulus under loading and reloading is defined as:

$$H_L = H_0 \cdot p' \cdot H_f \cdot (H_v + H_s) \cdot H_{DM} \quad (9)$$

$$H_f = (1 - \eta/\eta_f)^4 \quad (10)$$

$$\eta_f = (1 + 1/\alpha_f)M_f \quad (11)$$

$$H_v = 1 - \eta/M_g \quad (12)$$

$$H_s = \beta_0 \beta_1 \exp(-\beta_0 \xi) \quad (13)$$

$$H_{DM} = \left(\frac{\xi_{\max}}{\xi} \right)^{\gamma_{DM}} \quad (14)$$

$$\xi = p' \cdot \left[1 - \left(\frac{1 + \alpha_f}{\alpha_f} \right) \cdot \frac{\eta}{M_f} \right]^{1/\alpha_f} \quad (15)$$

where H_0 is the plastic modulus number; H_f , H_v , and H_s are the plastic coefficients; $\xi = \int |d\epsilon_s^q|$ is the accumulative plastic strain; and β_0 , β_1 , and γ_{DM} are model parameters.

The plastic modulus under unloading is defined as:

$$H_u = H_{u0} (\eta_u/M_g)^{-\gamma_u} \quad |\eta_u/M_g| < 1 \quad (16)$$

$$H_u = H_{u0} \quad |\eta_u/M_g| \geq 1 \quad (17)$$

The original model is mainly used for sand liquefaction analysis with a small effective confining pressure. However, the confining pressure varies from 0 to 3 MPa for high rockfill dams. In this paper, to better consider the effects of the wide range of confining pressures and the associated particle crushing on the response of rockfills in the dam, which differs from the response of sandy liquefaction sites, Eqs. 7, 8, 9, and (16) were modified as:

$$K = K_0 p_a (p'/p_a)^{m_v} \quad (18)$$

$$G = G_0 p_a (p'/p_a)^{m_s} \quad (19)$$

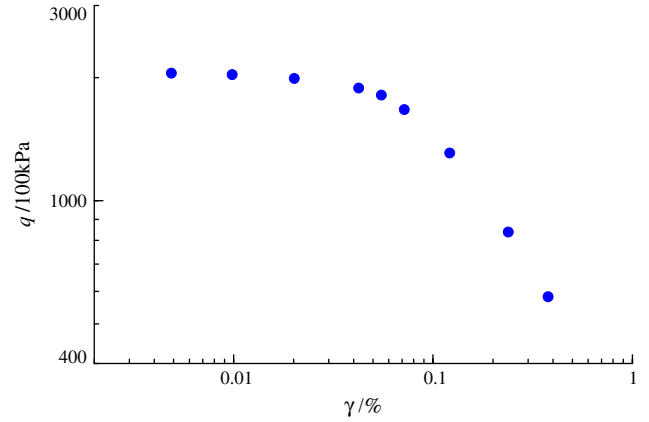
$$H_L = H_0 \cdot p_a \cdot (p'/p_a)^{m_l} \cdot H_f \cdot (H_v + H_s) \cdot H_{DM} \cdot H_{den} \quad (20)$$

$$H_u = H_{u0} \cdot p_a \cdot (p'/p_a)^{m_u} \cdot (\eta_u/M_g)^{-\gamma_u} \cdot H_{den} \quad |\eta_u/M_g| < 1 \quad (21)$$

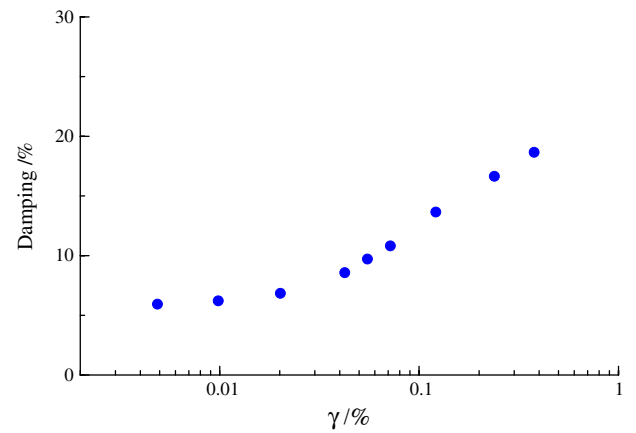
where p_a is the atmospheric pressure (100 kPa); H_{DM} is modified as $e^{(1-\eta/\eta_{\max})\gamma_{DM}}$; η_{\max} is largest value of the stress ratio attained; and $H_{den} = \exp(-\gamma_d \epsilon_v)$ is the densification coefficient, which takes into account the effects of cyclic hardening as proposed by Ling and Liu [24].

All of the exponents of K , G , H_L , and H_u were defined as 0.5 for sandy soils by Ling and Liu [24], which may not be appropriate for rockfill materials. In particular, rockfill materials exhibit considerable particle crushing under modest confining pressure and shear stress, while most sandy soil particles are much less crushable.

The modified model lack the capability of predicting the rockfill behaviors at small cyclic strains (10^{-6} – 10^{-4}) as given in Fig. 19a and b. However, the modified model can describe the modulus decreasing and the damping increasing with the shear strain increasing behaviors. Furthermore, the dynamic analysis emphasis on the large deformation of the Zipingpu CFRD during the strong excitation, which could be observed from the field damage (Fig. 4) and the simulated shear strain and volumetric strain (Fig. 13). The simulated cyclic stress–strain relationships and stress–path of typical elements of section 0 + 251 during the earthquake were given as Fig. 20a–c and Fig. 21a–c, it revealed that the dilatation under lower pressure and contraction characteristics under higher pressure of rockfill materials. The modified model could describe the characteristics, and is steady during dynamic analysis.



(a) Modulus ~ shear strain



(b) Damping ~ shear strain

Fig. 19. Simulated relationships of modulus and damping with shear strain (confining pressure: 500 kPa). (a) Modulus–shear strain and (b) damping–shear strain.

Appendix B

Interface. element and model behavior

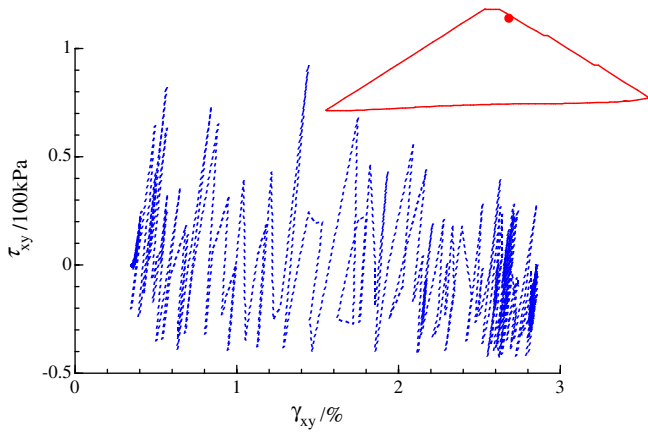
Goodman contact elements [28] without thickness, as depicted in Fig. 22, were applied between the face slabs and rockfills. The same elements were also applied to simulate the slab and peripheral joints. The relationship between force and displacement of a contact element is expressed as:

$$\begin{Bmatrix} \Delta F_{zx} \\ \Delta F_{zy} \\ \Delta F_{zz} \end{Bmatrix} = \begin{Bmatrix} k_{zx} & 0 & 0 \\ 0 & k_{zy} & 0 \\ 0 & 0 & k_{zz} \end{Bmatrix} \begin{Bmatrix} \Delta \delta_{zx} \\ \Delta \delta_{zy} \\ \Delta \delta_{zz} \end{Bmatrix} \quad (22)$$

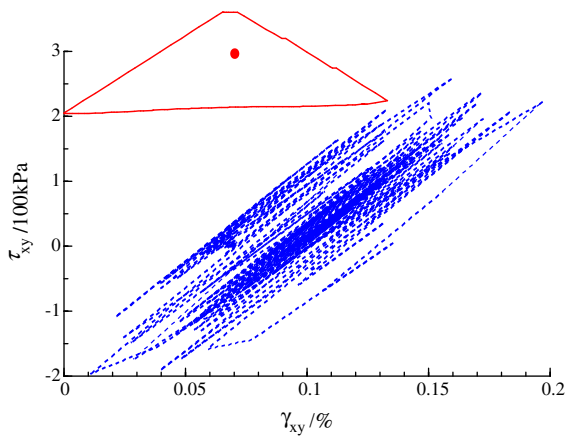
where ΔF_{zx} and ΔF_{zy} are the incremental shear stresses, k_{zx} and k_{zy} are shear stiffnesses, and $\Delta \delta_{zx}$ and $\Delta \delta_{zy}$ are incremental shear displacements in the two shear directions. ΔF_{zz} is incremental normal stress, k_{zz} is normal stiffness and $\Delta \delta_{zz}$ is the incremental normal displacement.

The pressure-dependent perfect elastoplastic interface model proposed was established for the interfaces between face slabs and rockfills and peripheral and construction joints for construction and seismic response analyses. The stiffness in the tangential and normal directions of the 3D contact element can be expressed as:

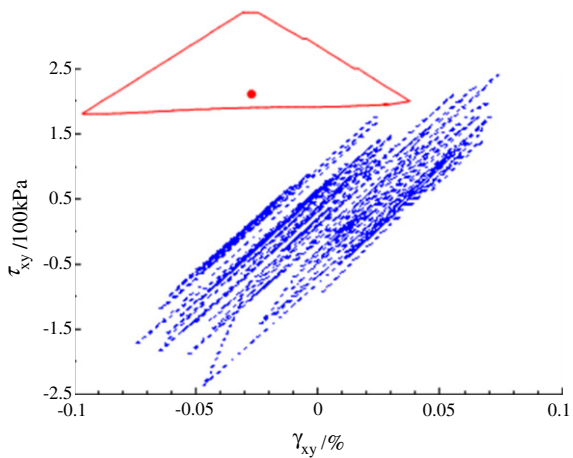
$$k_{zx} = k_1 p_a \left(\frac{\sigma_z}{p_a} \right)^n \quad (23)$$



(a) Element 15016 (depth: 4m)



(b) Element 15036 (depth: 80m)



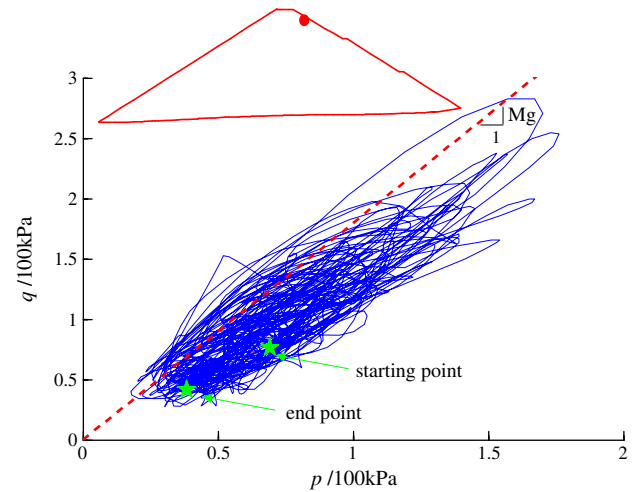
(c) Element 15048 (depth: 140m)

Fig. 20. Simulated cyclic stress–strain relationship of typical element of section 0 + 251 along the dam axial during the earthquake. (a) Element 15016 (depth: 4 m), (b) Element 15036 (depth: 80 m), and (c) Element 15048 (depth: 140 m).

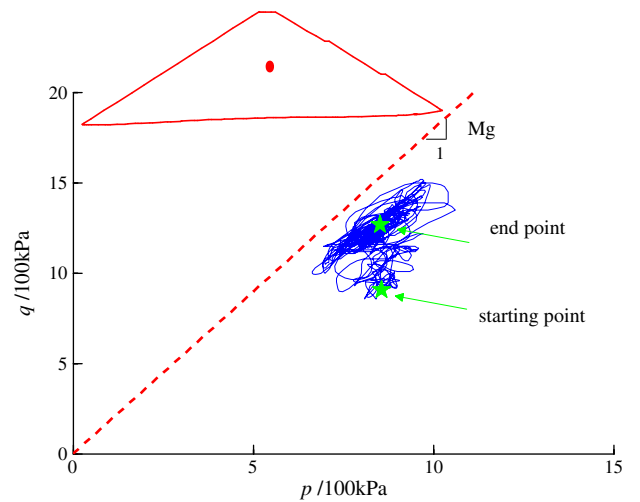
$$k_{zy} = k_1 p_a \left(\frac{\sigma_z}{p_a} \right)^n \quad (24)$$

$$k_{zz} = k_2 \quad \text{under compression} \quad (25)$$

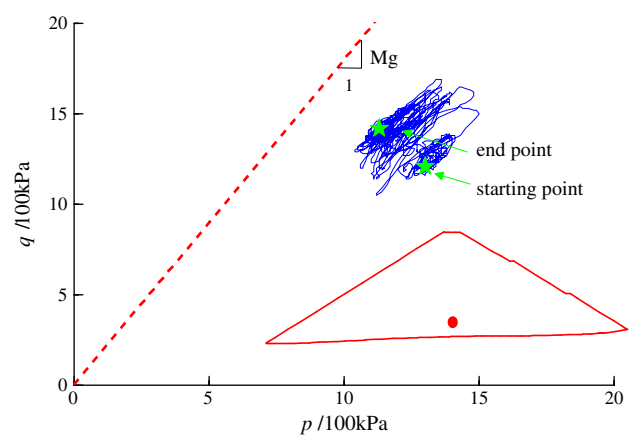
$$k_{zz} = 0 \quad \text{under tension} \quad (26)$$



(a) Element 15016 (depth: 4m)



(b) Element 15036 (depth: 80m)



(c) Element 15048 (depth: 140m)

Fig. 21. Simulated cyclic stress path of typical element during the earthquake. (a) Element 15016 (depth: 4 m), (b) Element 15036 (depth: 80 m), and (c) Element 15048 (depth: 140 m).

where p_a is the atmospheric pressure, k_{zx} and k_{zy} are tangential coefficients of shear stiffness in the two shear directions, k_1 is contact surface modulus factor, n is contact surface modulus exponent, R_f is failure ratio, φ is internal friction angle of the contact surface,

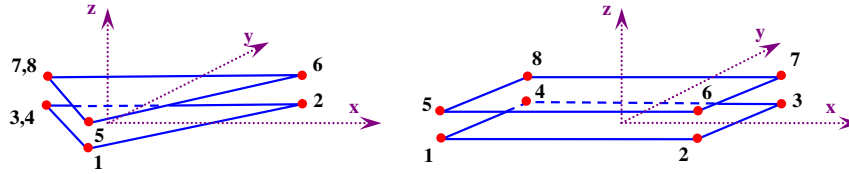


Fig. 22. Schematic diagram of the Goodman element.

σ_z is normal stress, τ_{zx} and τ_{zy} are shear stresses, c is interface cohesion and k_2 is the compressive stiffness.

References

- [1] Chen Shengshui, Huo Jiaping, Zhang Weiming. Analysis of effects of "5.12" Wenchuan earthquake on Zipingpu concrete face rock-fill dam. *Chin J Geotech Eng* 2008;30(6):795–801 (in Chinese).
- [2] Guan Zhicheng. Investigation of the 5.12 Wenchuan earthquake damages to the Zipingpu water control project and an assessment of its safety state. *Sci China Ser E – Tech Sci* 2011;52(4):820–34.
- [3] Mejia LH, Seed HB. Comparison of 2D and 3D analyses of earth dams. *J Geotech Eng ASCE* 1983;109(11):1383–98.
- [4] Gazetas G, Dakoulas P. Seismic analysis and design of rockfill dams: state of the art. *J Soil Dynam Earthquake Eng* 1992;11(1):27–61.
- [5] Uddin N, Gazetas G. Dynamic response of concrete-faced rockfill dams to strong seismic excitation. *J Geotech Eng* 1995;121(2):185–97.
- [6] Uddin N. A dynamic analysis procedure for concrete-faced rockfill dams subjected to strong seismic excitation. *Comput Struct* 1999;72:409–21.
- [7] Elgamal A-WM, Scott RF, Succarieh MF, Yan L. La Villita dam response during five earthquakes including permanent deformation. *J Geotech Eng Div ASCE* 1990;116(10):1443–62.
- [8] Elgamal A-WM. Three dimensional seismic analysis of La Villita dam. *J Geotech Eng Div ASCE* 1992;118(12):1937–58.
- [9] Succarieh M, Elgamal AW, Yan L. Observed and predicted earthquake response of La Villita dam. *J Eng Geol* 1993;34:11–26 (Elsevier Science Publishers).
- [10] Samiento N, Romo M, Marínez S, Marengo H. Seismic behavior of concrete-faced rockfill dams, considering a spatial variation of variation of motion along the rigid base. In: Proceedings of the 13th world conference on earthquake engineering. Paper no. 85; 2004.
- [11] Dakoulas P. Nonlinear seismic response of tall concrete faced rockfill dams in narrow canyons. *Soil Dynam Earthquake Eng* 2012;34(1):11–24.
- [12] Seiphoori A, Haeri SM, Karimi M. Three-dimensional nonlinear seismic analysis of concrete face rockfill dams subjected to scattered P, SV and SH waves considering the dam foundation interaction effects. *Soil Dynam Earthquake Eng* 2011;31(6):792–804.
- [13] Arici Yalin. Investigation of the cracking of CFRD face plates. *Comput Geotech* 2011;38(7):905–16.
- [14] Zhu Sheng, Yang Ge, Zhou Jianping, et al. *J Sichuan Univ (Eng Sci Ed)* 2010;42(5):113–9 (in Chinese).
- [15] Kong Xianjing, Zou Degao, Zhou Yang, et al. Earthquake damage analysis of Zipingpu concrete face rock-fill dam during Wenchuan earthquake. *J Dalian Univ Technol* 2009;49(5):667–74 (in Chinese).
- [16] Kong XJ, Zhou Y, Zou DG, et al. Numerical analysis of dislocations of the face slabs of the Zipingpu concrete faced rockfill dam during Wenchuan earthquake. *Earthquake Eng Vib* 2011;10(4):581–9.
- [17] Hardin BO, Drnevich V. Shear modulus and damping in soils. *J Soil Mech Found Div* 1972;98(7):667–92.
- [18] Newmark NM. Effects of earthquakes on dams and embankments. *Geotechnique* 1965;15(2):139–60.
- [19] Serff H, Seed HB. Earthquake induced deformation of earth dams. Berkeley: University of CA; 1976.
- [20] Mroz Z, Zienkiewicz OC. Uniform formulation of constitutive equations for clay and sand. In: Desai CS, Gallagher RH, editors. *Mechanics of engineering materials*. New York: Wiley; 1984. p. 415–50.
- [21] Pastor M, Zienkiewicz OC. Generalized plasticity and the modeling of soil behavior. *Int J Numer Anal Methods Geomech* 1990;14(3):151–90.
- [22] Pastor M, Zienkiewicz OC, Xu GD, et al. Modeling of sand behavior: cyclic loading, anisotropy and localization. In: Kolymbas D, editor. *Modern approaches to plasticity*. New York: Elsevier; 1993. p. 469–92.
- [23] Sassa S, Sekiguchi H. Analysis of waved-induced liquefaction of sand beds. *Geotechnique* 2001;51(2):115–26.
- [24] Ling HI, Liu H. Pressure dependency and densification behavior of sand through a generalized plasticity model. *J Eng Mech ASCE* 2003;129(8):851–60.
- [25] Ling HI, Yang S. Unified sand model based on the critical state and generalized plasticity. *J Eng Mech ASCE* 2006;132(12):1380–91.
- [26] Xu B, Zou Degao, Liu Huabei. Three-dimensional simulation of the construction process of the Zipingpu concrete face rockfill dam based on a generalized plasticity model. *Comput Geotech* 2012. <http://dx.doi.org/10.1016/j.comgeo.2012.03.002>.
- [27] Yu HY, Wang D, Yang YQ, et al. The preliminary analysis of strong ground motion records from the Ms 8.0 Wenchuan earthquake. *Earthquake Eng Vib* 2009;29(1):1–13 (in Chinese).
- [28] Goodman RE, Taylor RL, Brekke TL. A model for the mechanics of jointed rock. *J Soil Mech Found Div ASCE* 1968;94(SM3):637–59.
- [29] Zhang G, Zhang JM. Unified modeling of monotonic and cyclic behavior of interface between structure and gravelly soil. *Soils Found* 2008;48(2):237–51.
- [30] Zhang JM, Zhang G. Numerical modeling of soil–structure interface of a concrete-faced rockfill dam. *Comput Geotech* 2009;36(4):762–72.
- [31] Hofbeck JA, Ibrahim IO, Mattock AH. Shear transfer in reinforced concrete. *ACI J* 1969;2:119–28.
- [32] Li H, Liu XL. The critical tensile-shear failure and shear strength of concrete. *J Eng Mech* 1993;10(1):52–60 (in Chinese).
- [33] Jensen BC. Lines of discontinuity for displacement s in the theory of plasticity of plain and reinforced concrete. *J Mag Concr Res* 1975;92:143–50.
- [34] Mattock AH. Cyclic shear transfer and type of interface. *J Struct Div ASCE* 1981;107(10):1945–64.
- [35] Yu Yuzhen, Xie Liquan, Zhang Bingyin. Stability of earth–rockfill dams: influence of geometry on the three-dimensional effect. *Comput Geotech* 2005;32(5):326–39.
- [36] Zou Degao, Kong Xianjing, Xu Bin. User manual for geotechnical dynamic nonlinear analysis. Dalian: Institute of Earthquake Engineering, Dalian University of Technology; 2005.
- [37] Westergaard HM. Water pressures on dams during earthquakes. *Trans ASCE* 1933;98:418–33.
- [38] Bayraktar Alemdar, Murat Emre Kartal. Linear and nonlinear response of concrete slab on CFR dam during earthquake. *Soil Dynam Earthquake Eng* 2010;30(10):990–1003.
- [39] Nova RA. Constitutive model under monotonic and cyclic loading. In: Pande G, Zienkiewicz OC, editors. *Soil mechanics—transient and cyclic loads*. New York: John Wiley & Sons Ltd.; 1982. p. 343–73.
- [40] Zienkiewicz OC, Pande GN. Some useful forms of isotropic yield surface for soil and rock mechanics. In: Gudehus G, editor. *Finite elements in geomechanics*. New York: Wiley; 1977. p. 179–90.
- [41] Zou Degao, Zhou Yang, Ling Hoe I, Kong Xianjing. Dislocation of faced slabs of Zipingpu Concrete faced rockfill dam during Wenchuan earthquake. *J Earthquake Tsunami* 2012;6(2):1–17.